Scientific African 10 (2020) e00593

Contents lists available at ScienceDirect

Scientific African

journal homepage: www.elsevier.com/locate/sciaf

Development of MWCNTs/TiO_2 nanoadsorbent for simultaneous removal of phenol and cyanide from refinery wastewater

I. Kariim[a,b,*], A.S. Abdulkareem[a,b], J.O. Tijani[b,c], O.K. Abubakre[b,d]

[a] Chemical Engineering Department, Federal University of Technology, Minna, Nigeria
[b] Nanotechnology Research Group, Centre for Genetic Engineering and Nanotechnology, Federal University of Technology, Minna, Nigeria
[c] Chemistry Department, Federal University of Technology, Minna, Nigeria
[d] Department of Material and Metallurgy Engineering, Federal University of Technology, Minna, Nigeria

ARTICLE INFO

Article history:
Received 3 July 2019
Revised 2 July 2020
Accepted 23 September 2020

Keywords:
MWCNTs
TiO_2
Phenol
Cyanide
Nanoadsorbent
Characterization

ABSTRACT

The continuous discharge of untreated refinery wastewater containing pollutants into the water bodies have raised enormous concern on the safety of human, aquatic species and therefore calls for concerted efforts towards developing effective and sustainable treatment method. This study focused on the development of MWCNTs/TiO_2 nanoadsorbent for the removal of phenol and cyanide from refinery wastewater. MWCNTs was prepared via cracking of acetylene gas on nickel ferrites nanoparticles in a long tubular reactor. The MWCNTs and MWCNTs/TiO_2 nanoadsorbent were characterized for surface properties. HR-SEM and HR-TEM results revealed successive dispersion of TiO_2 on the pores of MWCNTs with average crystallite size of 37.32 nm and surface area of 360.66 m^2/g. The batch adsorption process revealed maximum removal of cyanide and phenol onto MWCNTs/TiO_2 adsorbent at 70 min, 0.3 g and 40 °C contact time, adsorbent dosage and temperature respectively. The experimental data were better described by Freundlich Isotherm and Pseudo second order kinetic model, an indication of multilayer adsorption. The values of the free energy change, (ΔG) were negatives which suggested the existence of strong bond formation between the adsorbates and the adsorbents. The study demonstrated that the developed MWCNTs/TiO_2nanoadsorbent is an excellent material for the sequestration of phenol and cyanide from refinery wastewater.

1. Introduction

The importance of potable water on human survival and sustenance including economy and health cannot be underestimated. Hence, water is an essential commodity for the safety of the human population [6]. However, the estimated death rate resulted from the consumption of polluted water containing diverse organic and inorganic contaminants such as phenol and cyanide was estimated to be between 10–20 million yearly [12]. The scarcity of clean water has resulted to drinking of

* Corresponding author.
E-mail address: k.ishaq@futminna.edu.ng (I. Kariim).

https://doi.org/10.1016/j.sciaf.2020.e00593

unconventional water sources with a consequential effects on health; a challenge affecting a population of over 0.78 billion of people around the globe. The water scarcity was projected to increase to about one-third of the world population [6]. Presently, the globe is facing tremendous challenges in meeting the growing demand for potable water as the accessible supplies of freshwater are diminishing due to both natural and artificial factors. Such factors include the population growth, extended droughts, rigorous health based regulations and competing demands amongst various users. There is need to monitor, control and regulate the introduction of pollutants into water bodies through the concern authorities to conserve the available freshwater for human consumption.

The introduction of bacteria, organic pollutants, micro-organism, industrial discharges or any form of compound that deteriorate the initial quality of water resulted in the formation of wastewater. Several reports have shown that series of contaminants are contained in the refinery wastewater such as heavy metals, hydrocarbons and phenol which cause severe damages to human system when diffused to water bodies without proper treatment methods [9,11,14,22]

Over the years, there has been continuous generation of phenol from petroleum refineries in large quantity which contributed to the formation of wastewater into the environment. According to Ilaboya et al., [10], phenol has been identified as the dominant organic contaminant in petroleum refineries which is difficult to degrade biologically. Cyanide is an immensely poisonous substance that is formed artificially and naturally. Cyanide has been extensively used in numerous applications in industries such as textile, plastics, photography, paints, electroplating, metal treatment, agriculture, mining and petrochemical industries [8,18,25]. Hence, there is need to design an integral wastewater mechanism to purify/remove heavy metals as well as organic pollutants from refinery wastewater before discharging it to the waterbodies to minimise environmental damages.

There are several methods available for the removal of contaminants from wastewaters. Such methods include, nanofiltration, reverse osmosis, hydroxide precipitation, coagulation and flocculation, solvent extraction, membrane separation, ion exchange, electrodialysis, and adsorption process [5,7,16]. Though membrane based processes such as ultrafiltration, microfiltration, nanofiltraton, and reverse osmosis are pressure-induced and are considered as an effective method of heavy metal removal but are costly to operate and maintain [1,26]. The high cost of operation and maintenance in addition to the cost of production therefore increases the production cost and hence, the selling price. Therefore, there is need to develop a low-cost, effective and efficient method of removing pollutants from refinery wastewater before being discharged to the water bodies.

Over the years, the application of adsorption process for the removal of heavy metals from industrial effluents and waterbodies has gained tremendous attentions from nanoscientists and engineers due to its effectiveness and efficiency coupled with the simplicity in maintenance and operation. The application of adsorption process for water purification entails the use of efficient adsorbent such as activated carbon, synthetic materials such as zeolite, carbon nanotubes, titanium dioxide, silicon (iv) oxide and cow dung. There are little findings on the application of Multiwalled carbon nanotubes supported titanium oxide nanoparticles, MWCNTs/TiO_2 composite adsorbent for the removal of cyanide and phenol from refinery wastewater. Although Nora et al., [17] findings indicated that the hybrid MWCNTs/TiO_2 shows improved properties compared to the individual constituents. Furthermore, the findings of Mombeshora et al., [15] revealed that the nanocomposite of MWCNTs/TiO_2 has shown an improved efficiency to bare titanium oxide nanoparticles and MWCNTs in isolation when applied in various area of applications such as electrochemistry, energy storage, energy conversion, photo-catalysis and dye induced solar [3,13,21].

In this present research work, MWCNTs was developed in a CVD reactor. The synthesized MWCNTs was blended with the developed TiO_2 nanoparticles synthesized via green synthesis route. The MWCNTs/TiO_2 nanoadsorbent was used for the adsorption of cyanide and phenol from refinery wastewater via batch adsorption process. The kinetic, isotherm and thermodynamic studies describing the adsorption of phenol and cyanide on to the pores and surfaces of the adsorbents were investigated.

2. Methodology

2.1. Material

All the chemicals and gases used are of analytical grade with percentage purity of 99.99 %. The *Taminaliacatappa* (almond plant) was collected from Bosso Campus, Federal University of Technology, Minna, Niger State, Nigeria. Prior to the extraction process, the plant samples were washed with distilled water to remove sand and other dirt then dried at 30 °C under room condition to remove moisture content. The catalyst used (Fe-Ni/Al_2O_3) was obtained from Nano Research Group of Centre for Genetic Engineering and Nanotechnology, Federal University of Technology, Minna, Nigeria with its properties reported by Kariim et al., 2015.

2.3. Synthesis of MWCNTs in a CVD reactor

A known weight (1.0 g) of the developed nickel ferrite nanoparticles supported on alumina (Fe-Ni/Al_2O_3) was placed in a quartz boat positioned at the centre of the quartz tube reactor. The CVD was heated at 10 °C/min under the flow of an inert gas, nitrogen at a flow rate of 30 mL/min. The flow of the carbon source (acetylene) is feed into the reactor at 250 mL/min flow rate immediately the reaction temperature of 600 °Cis attained. The reaction is maintained at a controlled reaction

time of 45 min for the catalytic degradation of the carbon source. Immediately the reaction time is attained, the flow of the carbon source is truncated while the carrier gas flowrate is lowered to purge and cooled the system to room temperature. The produced MWCNTs was therefore removed and kept in sample bottle for further use.

2.4. Purification of as-synthesised MWCNTs

A known quantity of the as produced MWCNT (1.0 g) was weighed from the bulk of the MWCNTs produced and was purified by adding 30:70 v/v of sulfuric acid and distilled water in a beaker, heated and stirred using a magnetic stirrer at a temperature of 50 °C for 40 min to remove any residual impurities associated with the produced carbon nanotubes. The produced mixture was allowed to settle down, cooled then filtered with continuous washing until a pH of 7 was attained. The residue, purified MWCNTs was collected then dried at a temperature of 100 °C for 7 h to remove water content.

2.5. Extraction of plant extract from of Taminaliacatappa leaves

The *Taminaliacatappa* plant leaves sourced was dried to remove/reduce any water content present in the bulk of the material. The dried leaves were grinded using mortar and pestle then sieved via 1.70 mm mesh size. 100 g of the sieved leave was then transferred into a beaker that contains 300 mL of distilled water and allowed to stand for 24 h. The mixture was filtered via a Whatman filter paper and the filtrate was collected while the residue was discarded.

2.6. Production of TiO_2 nanoparticles

The leave extract obtained was employed as a reducing agent for the reduction of titanium tetraisopropoxide to TiO_2 nanoparticles. About 100 mL of 1.5 N of titanium tetraisopropoxide was prepared and placed immediately on a magnetic stirrer. 8 mL of the leave extract was added dropwise into the 100 ml of 1.5 N of titanium tetraisopropoxide under continuous stirring using magnetic stirrer. The stirring continues for a period of 3 h at room temperature with a formation of gelatinous precipitate. The developed nanoparticles were separated from the solution by filtration using Whatman filter paper, dried at a temperature of 80 ^{0}C in an air oven for 12 h to remove moisture content. The dried nanoparticles were then calcined at a temperature of 400 ^{0}C for 2 h to obtain TiO_2 nanoparticles.

2.7. Development of MWCNTs/TiO_2 nanoparticles

MWCNTs/TiO_2 adsorbent was developed by impregnation method. A weight ratio of 80:20 wt% (g/g) of the MWCNTs to TiO_2 was stirred in 50 ml of distilled water for a period of 24 h. The resulting mixture was dried at a temperature of 120 °C for 10 h. The dried MWCNTs/TiO_2 was grinded, sieved through a 150 mM sieve size.

2.8. Characterization of the prepared MWCNTs, TiO_2 and MWCNTs/TiO_2 nanomaterials

The surface area, surface functional group, surface morphology/elemental composition, internal morphology (wall structure) and crystallinity were determined using BET (NOVA 4200e Quantachrome Instruments analyzer, samples were degassed at 250 °C then analysed in Nitrogen environment), FTIR(Perkin Elmer Frontier FTIR Spectrometer, spectra of the sample were obtained within 400 to 4000 cm^{-1} with a 1 cm^{-1} resolution operated 0.125 $cm^{-1}s^{-1}$), HR-SEM/EDS (Joel JEM 100S HRSEM operating at 80 kV), HR-TEM (Philips CM20FEG operating at 200 keV) and XRD (PW1800 diffractometer, 5 ^{o}/min scanning speed, 55 mA generator settings and 40 kV, using CuKα node material).

2.9. Adsorption studies

2.9.1. Effect of contact time on the adsorption of cyanide and phenol

The effect of contact time on the adsorption capacity of the developed adsorbent in the removal of cyanide and phenol was carried out. During this study, 0.05 g of the adsorbents was added to 50 mL of the refinery wastewater contained in a conical flask placed in a water bath shaker at 200 rpm under room temperature. The experiment was conducted for varied contact time of 10,20,30,40,50,60,70 and 80 min while the dosage, temperature and the agitation speed were kept constant. The obtained dispersions were then filtered, the clear solutions were collected and thereafter, the concentration of the cyanide and the phenol were determined via titrimetric and spectroscopy techniques respectively.

2.9.2. Effect of adsorbent dosage on the adsorption of cyanide and phenol

The effect of adsorbent dosage was carried out by varied the mass of the nanoadsorbent during the batch adsorption process. A known mass of 0.05,0.1,0.15,0.2,0.25,0.3 and 0.35 g of the adsorbents were added to 50 mL of the refinery wastewater contained in a 100 mL conical flask placed in a water bath shaker at 200 rpm under room temperature and equilibrium time. The obtained dispersions were then filtered, the clear solutions were collected and thereafter, the concentration of the cyanide and the phenol were determined via titrimetric and spectroscopy techniques respectively.

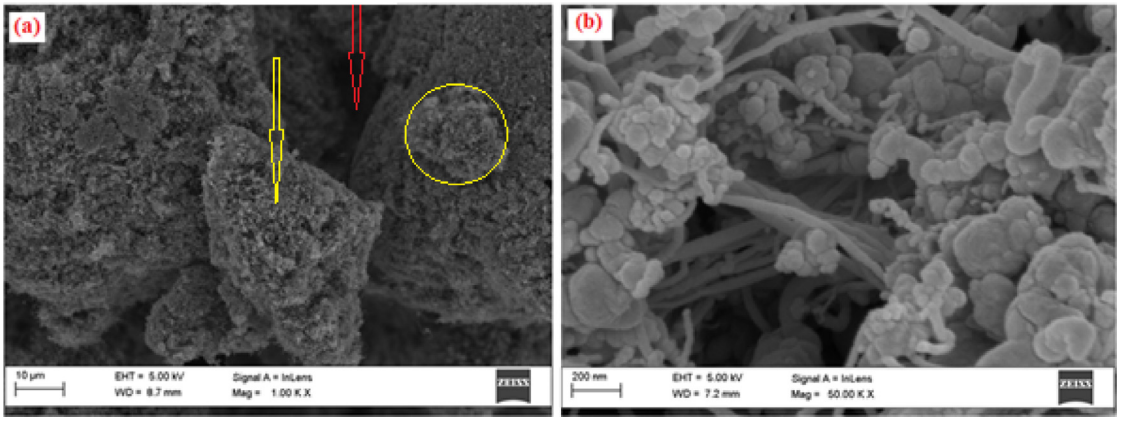

Fig. 1. : HR-SEM Micrograph of as-synthesized MWCNTS

2.9.3. Effect of temperature on the adsorption of cyanide and phenol

The study was aimed at determining the thermodynamic behaviours of the adsorption process by varying the temperature while other factors were kept constant. A known weight (0.35 g) of the adsorbents were weighed and added into the 50 mL of the refinery wastewater contained in a 100 mL conical flask placed in a water bath shaker at 200 rpm maintained at equilibrium time. The temperature of the adsorption process was varied from 30 to 70 °C while the volume of wastewater, the dosage, agitation speed and the contact time were kept constant. The obtained dispersions were then filtered, the clear solutions were collected and thereafter, the concentration of the cyanide and the phenol were determined via titrimetric and spectroscopic techniques respectively**.**

2.10. Data analysis

The adsorption capacity of the nanoadsorbents were determined using the mass balance relationship presented in Eq. 1 [19] while the percentage cyanide and phenol removalwas determined using Eq. 2.

$$Q = \frac{V(Co - Ce)}{W} \times 100 \tag{1}$$

$$\%\ Removal = \frac{(Co - Ce)}{Co} \times 100 \tag{2}$$

Where C_o, C_e, V, W and Q represent the initial ion concentration before the adsorption process (mg/L), the final ion concentration after the adsorption process (mg/L), Volume of the wastewater (L), mass of adsorbent (mg) and amount of adsorbed ions onto the adsorbent (mg/g) respectively.

3. Results and discussion

3.1. Characterization of the as-synthesised MWCNTs

Fig. 1 depicts the HR-SEM micrograph of the as-synthesized multiwalled carbon nanotubes produced using the sourced Fe-Ni supported on alumina catalyst and revealed irregular nature of the synthesized materials with varied MWCNTs sizes.

From Fig. 1a, there is an indication of the carbon nanotubes growth on the particles of the catalysts used (this is indicated with circle on Fig. 1a). Furthermore, the formation of coiled-shape MWCNTs was also observed in Fig. 1b. The nature of the MWCNTs synthesised was found to be dense with coiled ends.

The elemental content of the as-synthesized MWCNTS depicted in Fig. 2 showed the presence of five elements constituting the bulk of the as-synthesized MWCNTs produced.

These elements include; Carbon (C), Oxygen (O), Aluminium (Al), Iron (Fe) and Nickel (Ni) with percentage composition of 77.31,12.28,9.35,0.44 and 0.62 % respectively. It was observed that carbon, C has the highest percentage composition in the bulk of the as-synthesized MWCNTs. The possible reason for the highest percentage composition possessed by carbon could be traced to high percentage conversion of acetylene gas during the nucleation process. The percentage carbon obtained is relatively close to the observed quantity reported by Aliyu [2] who worked on the synthesis of CNTs using Fe-Ni/kaolin in a CVD reactor.

Moreover, the presence of oxygen with 12.28 % could be linked to the oxide of metals present after the catalytic cracking process. Also, the percentage composition of Al could be linked to the support material used for catalysts development. The ratio of Iron to Nickel was observed to be 1:1.4. The observed ratio was close to the adopted weight percent of 1:1 used during the catalyst preparation stage.

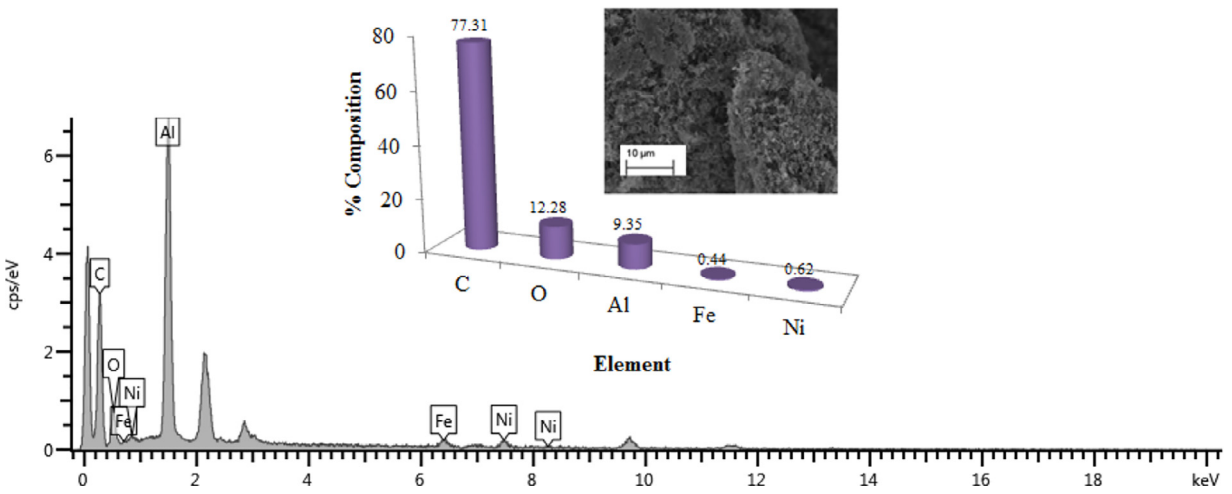

Fig. 2. : EDS Spectrum of as-synthesized MWCNTs

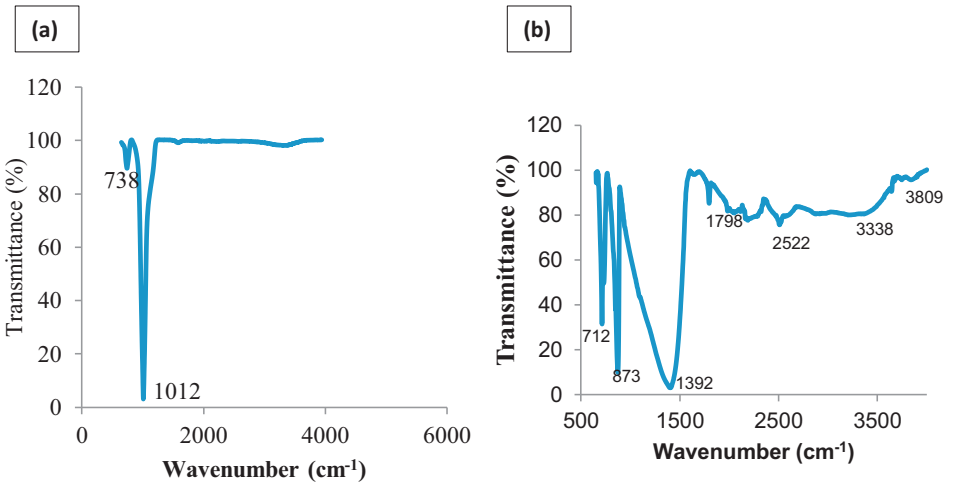

Fig. 3. : FTIR Spectrum of (a) as-synthesized MWCNTs (b) purified MWCNTs

The surface functional group present on the as-synthesized MWCNTS produced via the catalytic cracking of acetylene gas was determined using the Fourier Transform Infrared Spectroscopy (FTIR) and the spectra is shown in Fig. 3.

Fig. 3a shows the presence of two pronounced functional groups with the peaks around 738 and 1012 cm^{-1}which fall within the finger prints region. These wavenumber of 738 and 1012 cm^{-1}were assigned to C–O and C–C bending bonds in the as-synthesized MWCNTS respectively. The purification method was expected to introduce functional groups such as -COOH into the surface of the carbon nanotubes; the nature of the introduced functional group is a function of the nature of the acid used and the purification technique adopted. Fig. 3(b) revealed the presence of absorption bonds at the wavenumber of 3338 and 1798 cm^{-1} which correspond to O–H bonding on the surface of the MWCNTs. The wavenumber of 3809 cm^{-1} was associated to the presence of –OH bond. Furthermore, the presence of C=C bond was observed at the wavenumber of 1392 cm^{-1} which exists due to incomplete acetylene conversion during the nucleation process. The peak at the wavenumber of 712 cm^{-1} indicates the presence of O–C bond in the purified MWCNTs. The possible occurrence of this peak could be linked to the oxidation process which might have occurred in the drying process employed during the purification process.

The internal microstructural arrangement of the as-synthesized MWCNTS was determined by high resolution transmission electron microscope (HRTEM) and micrographs were shown in Fig. 4(a-c).

Fig. 4c shows that the as-synthesized carbon nanotubes is multi-walled in nature with the external diameter in the range of 4.76 nm to 46.81 nm. The diameter and length of the encapsulated metallic catalyst material onto the tube wall of the as-synthesized MWCNTs were determined to be 8.40 nm and 20.67 nm. The lattice fringes was estimated to be 0.22 nm which is an evidence for the formation of graphitic carbon hence, corresponds to the (002) indexing as indicated on the XRD result (Fig. 3b). From Fig. 4a, the black spot as indicated with red arrow shows the presence of catalyst particles

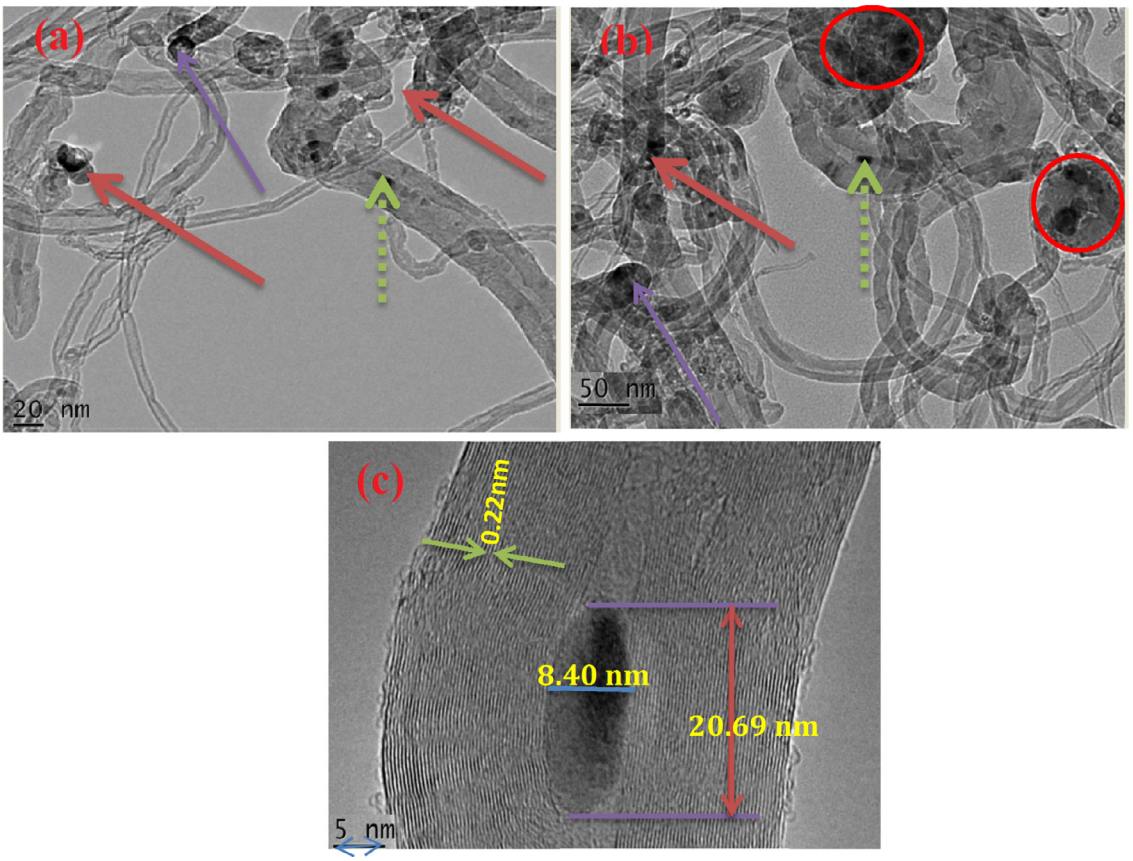

Fig. 4. : HR-TEM Micrograph of the as-synthesized MWCNTs

attached to the wall of the MWCNTs grown. This further shows that the catalyst material is not used up in the course of the catalytic cracking process. Also, the green arrow indicated in Fig. 4(a) and (b) further implied that the catalyst materials were encapsulated within the wall of the as-synthesized MWCNTs produced. Several growth methods have been postulated in the synthesis of MWCNTS in a CVD reactor. In this present study, the base growth mechanism was observed as depicted by the purple arrows on both the Fig. 4(a) and (b).

The SAED analysis was performed to determine the crystal lattice and d-spacing of the as-synthesized MWCNTs and the results are depicted in Fig.5 (a) and (b).

The result as shown in Fig. 5(a) has four distinct rings with radii 0.47,0.23,0.18 and 0.14 nm corresponding to FCC, BCC, FCC and FCC crystal lattice. The (002) indexing of the first ring represents the graphitic carbon. Critical observation of the ring, Fig. 5(a) shows the presence of dull rings which is a possible indication of presence of amorphous materials. The single pattern of a SAED as depicted in Fig. 5 (b) is made up of several components of spots that form the ring, clearer than those formed in Fig. 4(a). These rings are closely but symmetrically formed with a unique centre. The crystallite radii on the rings were determined to be 0.400,0.218,0.170 and 0.126 nm from the innermost to the outermost ring. The purification process was found to have no effect on the phase changes on the crystals of the multiwalled carbon nanotubes after the process as compared to the result depicted on Fig. 5(a). Hence, the employed purification process is highly suitable for controlled metallic particle removal without introducing any changes into the crystallite phase in the bulk of the MWCNTs.

The surface morphology of the purified MWCNTs was determined with the aid of a high resolution transmission electron microscope (HR-SEM). The HR-SEM micrograph of the purified MWCNTs is depicted in Fig. 6(a-b).

Fig. 6(a-b) revealed the presence of highly populated strand of MWCNTs with short length while Fig. 11b shows the formation of disjointed branch tube on the wall of the nanotubes due to the nucleation process. Details observation of the tubes indicate that the diameter of the purified tubes were irregular which could be linked to the variation of catalyst's diameter.

The internal morphology of the purified MWCNTs was determined using of High Resolution Transmission Electron Microscope (HRTEM) and the micrographs are depicted in Fig. 7a and b.

Fig. 7a shows that high percentage of the metallic catalyst in the form of agglomerate which has been removed except in those entrapped within the tube of the MWCNTs. The Inter-planner d-spacing of the lattice fringe was estimated to be 0.27 nm which agrees with the values reported for graphitic MWCNTs formation. The internal and external diameters of the

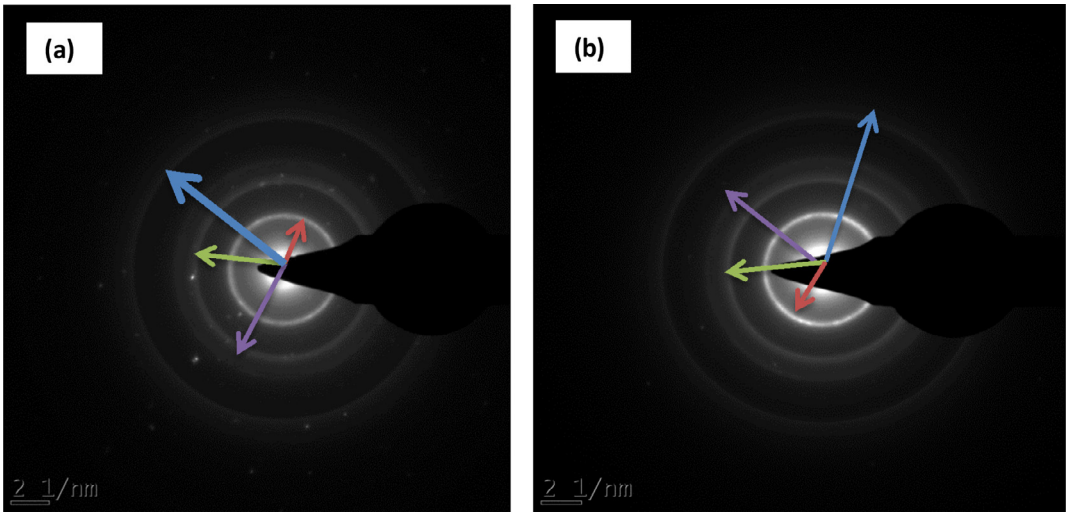

Fig. 5. SAED pattern of (a) as-synthesized (b) purified MWCNTs

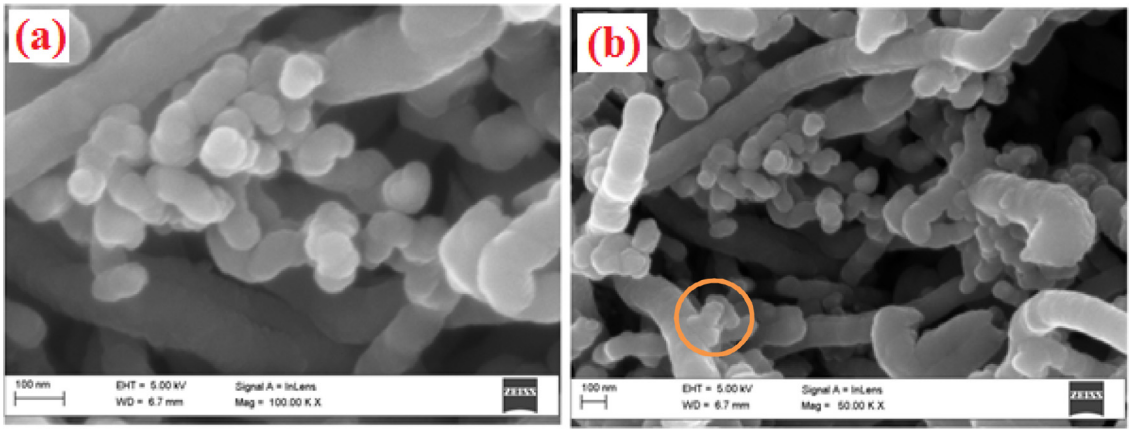

Fig. 6. HR-SEM micrograph of purified MWCNTs (a) High (b) Low magnification

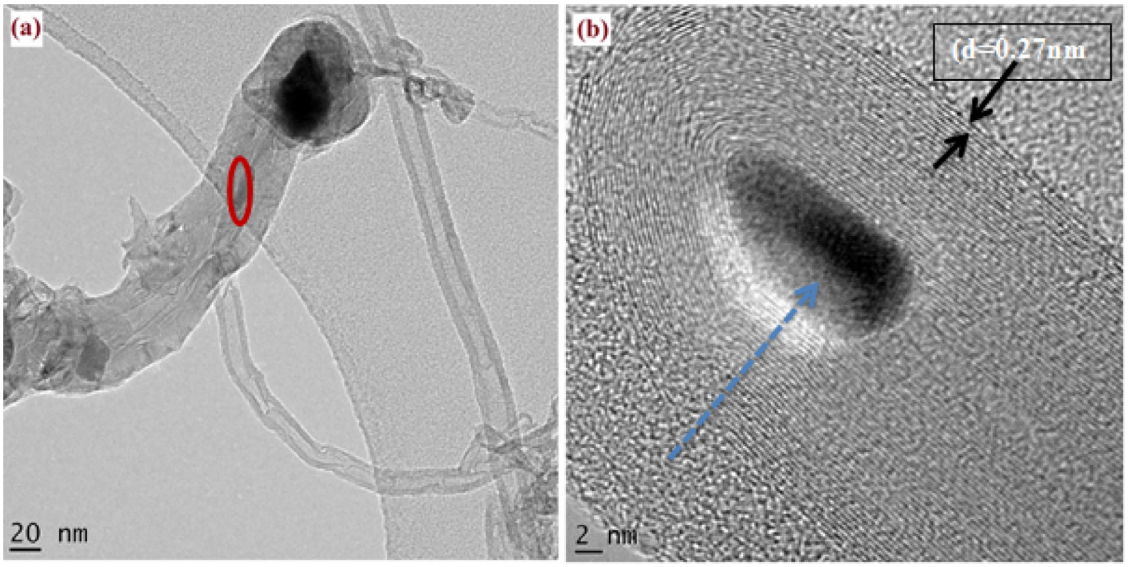

Fig. 7. HR-TEM micrograph of purified MWCNTs

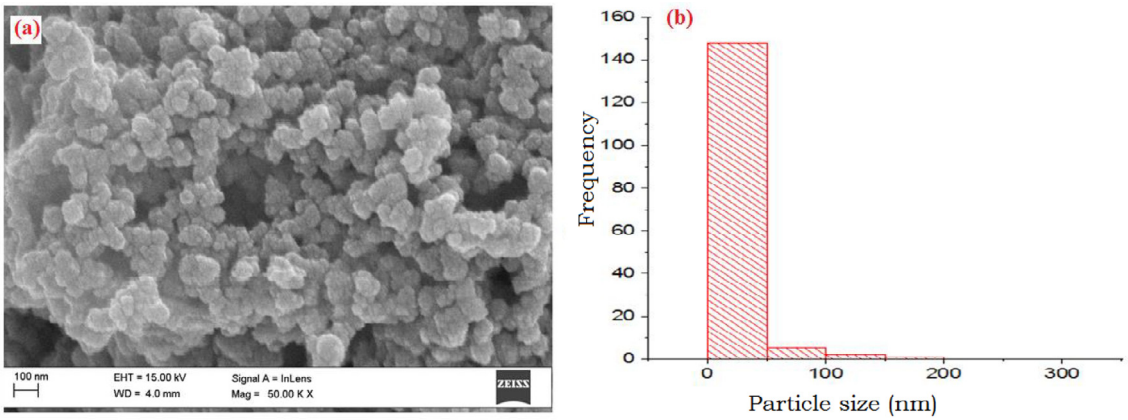

Fig. 8. (a) HR-SEM micrograph of TiO_2 nanoparticles developed (b) Particle size distribution of the TiO_2 nanoparticles produced

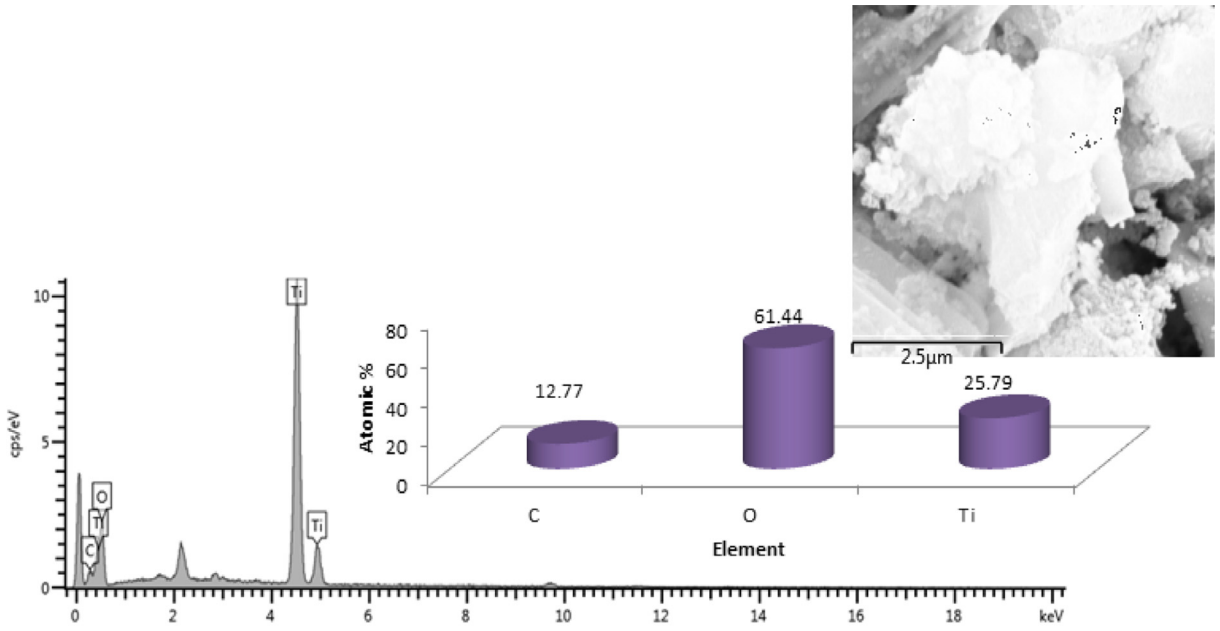

Fig. 9. EDS Spectrum and the elemental composition of the developed TiO_2 nanoparticle produced

purified MWCNTS were found to be 8.89 nm and 18.57 nm respectively. The tube opening of the purified MWCNTS, Fig. 7b also revealed that the hollow cavity of the MWCNTs was produced. It was further observed that the preence of impurities on the surfaces of the carbon nanotubes were negligible compared to that of the as-synthesized MWCNTs depicted in Fig. 4(a-c).

The surface morphology of the developed TiO_2 was investigated by HRSEM and the micrograph is shown in Fig. 8(a) while the particle size distribution is presented in Fig. 8(b).

Fig. 8(a) revealed the presence of dense agglomerated spherical particles with particle sizes of 1.59 to 200 nm which were stony in nature. The observable stony nature of produced nanoparticles were similar to those reported by Bani et al. [4].

The result of the EDX analysis of the developed TiO_2 is as shown in Fig. 9.

Fig. 9 revealed the presence of three distinct elements; C, O and Ti with atomic percent of 12.77, 61.44 and 25.79 respectively. The Carbon, C in the result depicted may originated from the plant extract or the adhesive tape used for the SEM analysis. Also, the presence of titanium at varied energy level implies its existence in variable oxidation states o +3 or +4 in the bulk of the nanomaterials.

The XRD analysis was used to determine the crystallinity, crystallite particle size as well as phase identification in the developed TiO_2 nanoparticle produced. The result of the XRD analysis is as presented in Fig. 10.

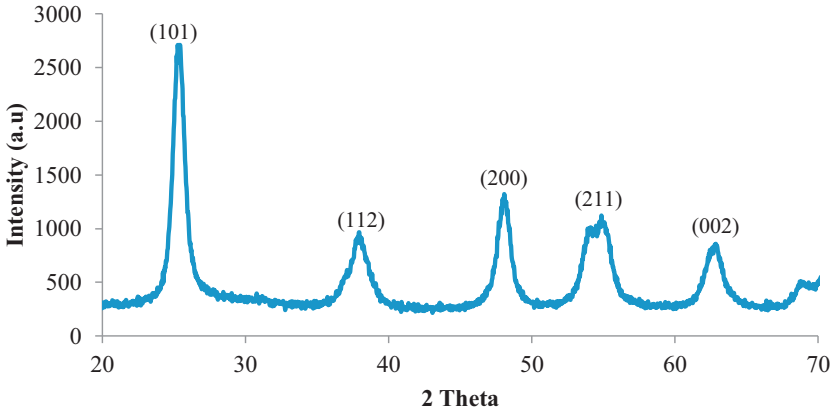

Fig. 10. XRD Spectral of the developed TiO_2 nanoparticles

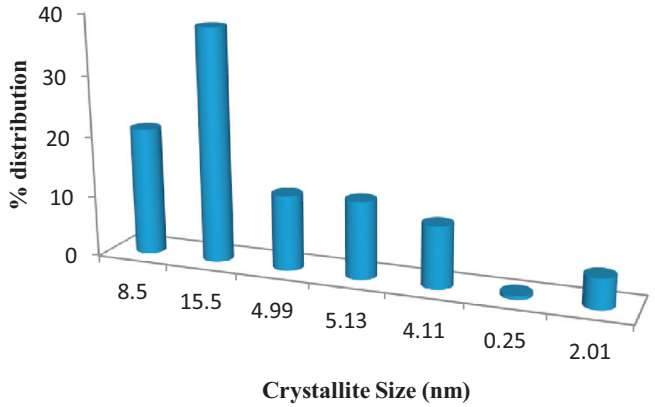

Fig. 11. Crystallite size distribution of the produced TiO_2 nanoparticles

The XRD pattern in Fig. 10 depicts several diffraction peaks in the bulk of the nanomaterial. The peaks were pronounced at the diffraction angle of 25.35, 37.92, 48.10, 54.75, 62.81, 70.24 and 75.26 º with miller indexes of 101, 112, 200, 211, 211 and 002 respectively. The highest reflection peaks were pronounced at the diffraction angles of 25.35 and 48.10 º which indicate the dominance of anatase type of TiO_2 nanoparticles while the peak at 54.75 º indicates the presence of rutile phase of the produced TiO_2 nanoparticles. This observation is in accordance with the report of Thamaphat *et al.* [24].

Based on the identified main peaks in the XRD spectral from Fig. 10, the crystallites sizes of the developed TiO_2 were calculated using Scherrer equation (Eq. 3) and the result is shown in Fig. 11. The crystallite sizes were found to be in the range of 0.25-15.50 nm

$$D = \frac{0.9\lambda}{\beta \, \mathrm{Cos}\, \theta} \tag{3}$$

Where λ represents x-ray wavelength, θ is the Bragg's diffraction angle, β the Full Width at Half Maximum (FWHM) and D is the crystallite size.

Furthermore, the average crystallite sizes were found to be 5.78 nm. This value is lower compared to the value reported by Rao et al., [23]. The reason could be attributed to the nature of reducing agent used and the synthesis condition.

The microstructure and the crystalline nature of the developed MWCNTs/TiO_2 nanoadsorbent were investigated using HRTEM and the HRTEM images are shown in Fig. 12(a-d).

The HRTEM result as presented (Fig. 12a) shows the extent of TiO_2 nanoparticles distribution on the surface of the MWCNTs. The spongy-like nature of the developed nano-adsorbent is evident on Fig. 19 (a); an indication of even distribution of the TiO_2 nanoparticles on the surface of the MWCNTs. Interestingly, the encapsulation observed in Fig. 12(b) was linked to the accompanied metallic catalyst formation during the nucleation process while the TiO_2 nanoparticles were obvious on the surface of the MWCNTs. To further reveal the internal make-up of the developed MWCNTs/TiO_2 nanocomposite produced, the external and the internal diameter of the material were estimated to be 28.17 and 10.92 nm respectively.

The quantitative analysis of these constituents was done using EDX as shown in Fig. 13a.

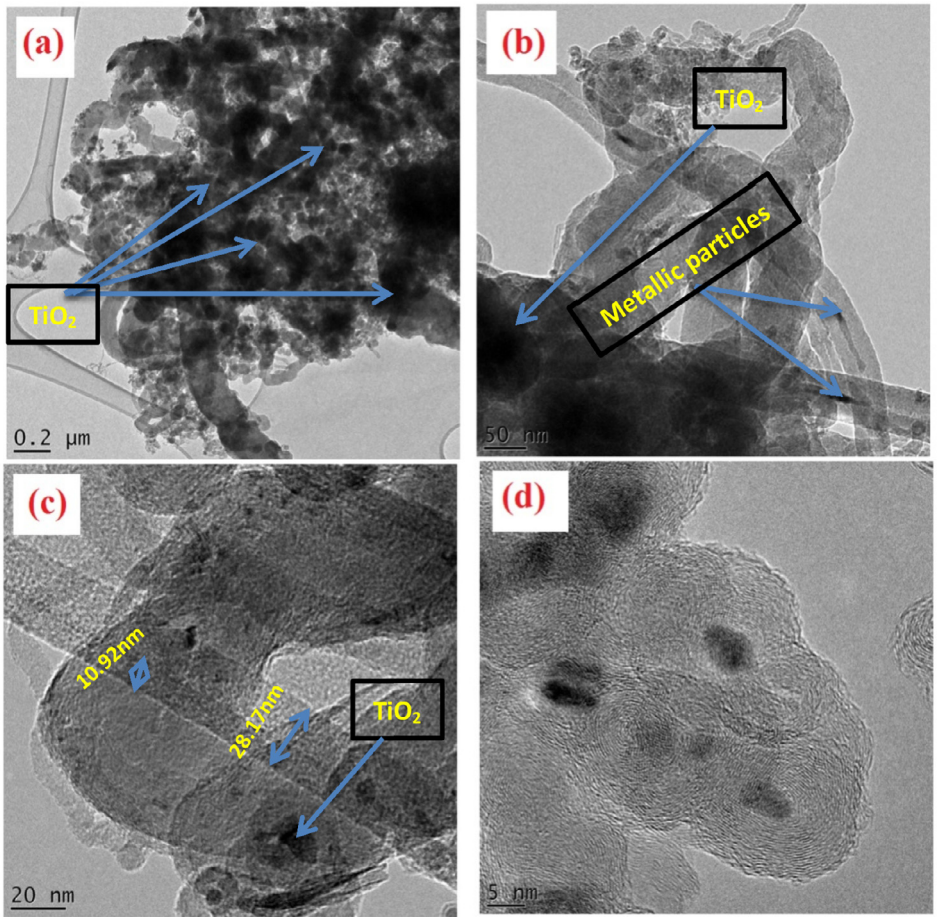

Fig. 12. HR-TEM micrograph of the developed MWCNTs/TiO_2 nanocomposites at varied magnification

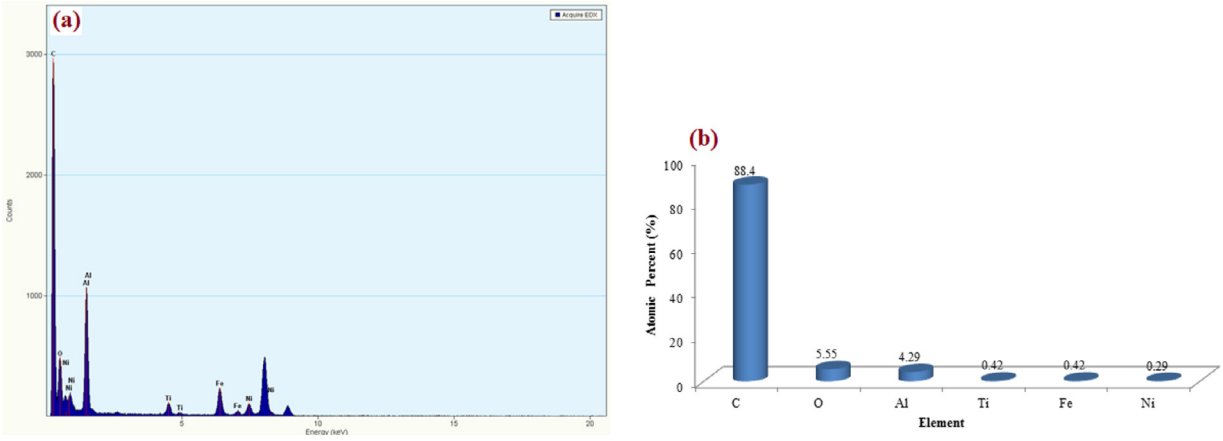

Fig. 13. (a) EDS spectrum and (b) Elemental composition of the developed MWCNTS/TiO_2 nanocomposite

The EDS spectra shown in Fig. 13(a) depicts the presence of Al, Fe, Ni, C and Ti elements at varied energy level. The Fe and Ni originated from the metal salt precursor used. Noticeably, carbon, (C) appearance is linked to the graphitized MWCNTs used as the base material for the composite development. It is worthy to note that the presence of the Fe and Ni suggests partial removal by the acid used during the purification process.

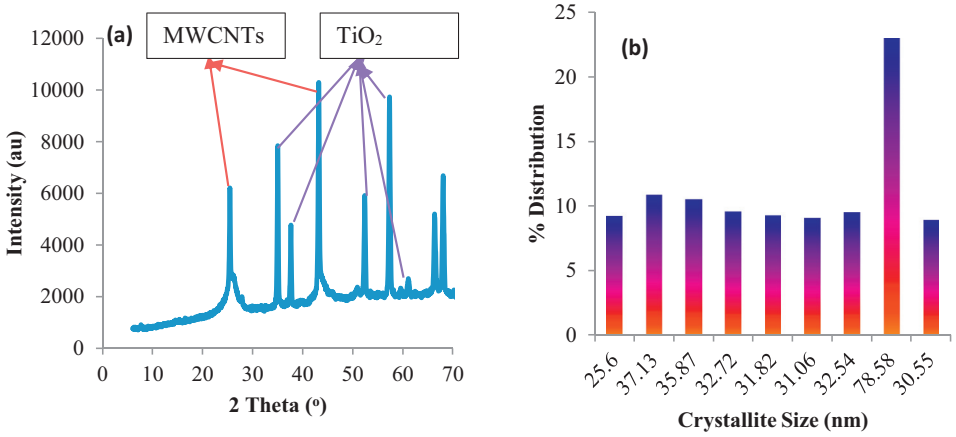

Fig.14. : (a) XRD Spectral (b) crystallite particle size distribution of the developed MWCNTs/TiO_2 nanoadsorbent.

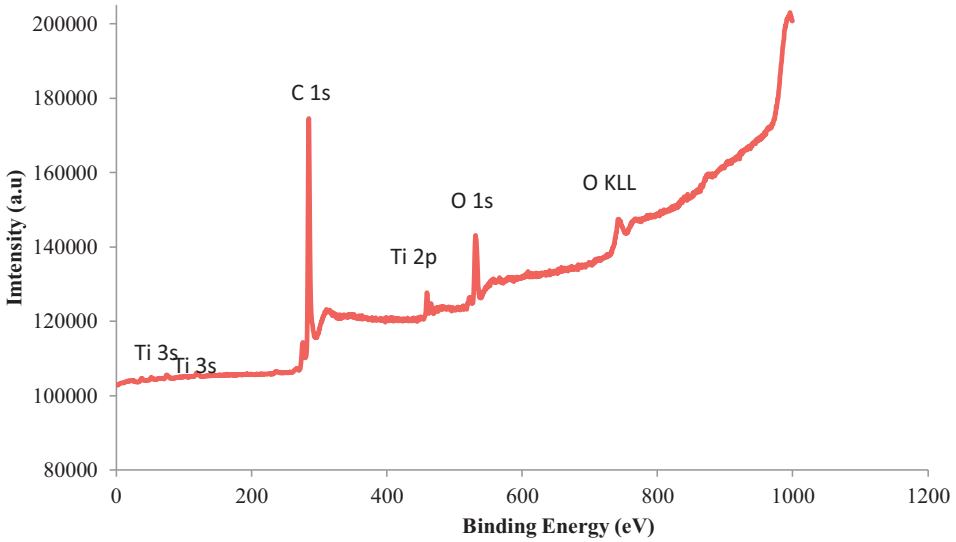

Fig. 15. XPS spectrum MWCNTs/TiO_2 nanoadsorbent

Fig. 14 revealed the XRD pattern of MWCNT/TiO_2 nanoadsorbent developed which shows the presence of several peaks indicating the diffraction angle of the constituents compounds as contained in the developed MWCNT/TiO_2 nanocomposites. The peaks observed at 25.

In Fig. 14(a), there were observable diffraction peaks at the 2 theta values of 25.45, 34.99, 37.66, 43.25, 53.41, 57.35, 66.47, 68.09 and 76.76 °. The diffraction angles at the 2 theta values of 25.45 and 43.25 °C correspond to the graphitic nature of the MWCNTs used for the composite development. Furthermore, the retention of these peaks is an indication that the employed methodology did not affect the phase of the base material. The crystallite particle size of the MWCNTs/TiO_2 nanoadsorbent is shown in Fig. 14(b). The crystallite size distribution as depicted in Fig. 14(b) shows that the crystallite sizes ranges from 30.55–78.58 nm with average size of 37.32 nm.

The XPS spectra of the developed MWCNTs/TiO_2 nanoadsorbent are shown in Fig. 15.

XPS analysis was carried out to measure the oxidation state elements present on the surfaces of the developed adsorbent. The sputtered MWCNTs/TiO_2 depicts the presence of C (285.0 eV), O (532.5 eV), and Ti (460.1 eV) though at varied binding energy level. The presence of Ti at the binding energy of 460.1 eV suggests the formation of TiO_2 nanoparticles. Hence, the XPS results depicts that the TiO_2 nanoparticles was successfully anchored on the surfaces of the MWCNTs material.

The surface area of the developed adsorbent were determined and presented in Table 4.

From Table 3, the P-MWCNTs was found to possess high surface area as compared to 178 m^2/g reported by [20] as the surface area of commercial MWCNTs and those of the average surface area of a MWCNTs, taking into consideration, the uncertainty, the thickness as well as the diameter of the tubes. The blending of MWCNTs with TiO_2 resulted to a slight reduction in the surface area of the resulting composite to 360.67 m^2/g. The results of various characterization show that

Table 3
Surface area, pore size and pore volume of the developed adsorbents

Adsorbent	BET surface area (m^2/g)	Pore Volume (cc/g)	Pore size (nm)
MWCNTs	393.32	0.26	2.01
TiO_2	410.31	0.45	3.02
MWCNTs/TiO_2	360.67	0.21	1.98

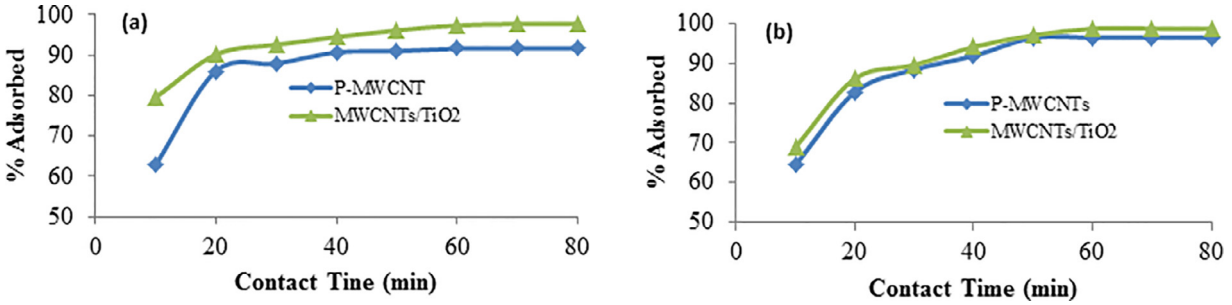

Fig. 16. Effect of contact time on the percentage removal of (a) Cyanide and (b) Phenol onto MWCNTs and MWCNTs/TiO_2 nanodsorbents.

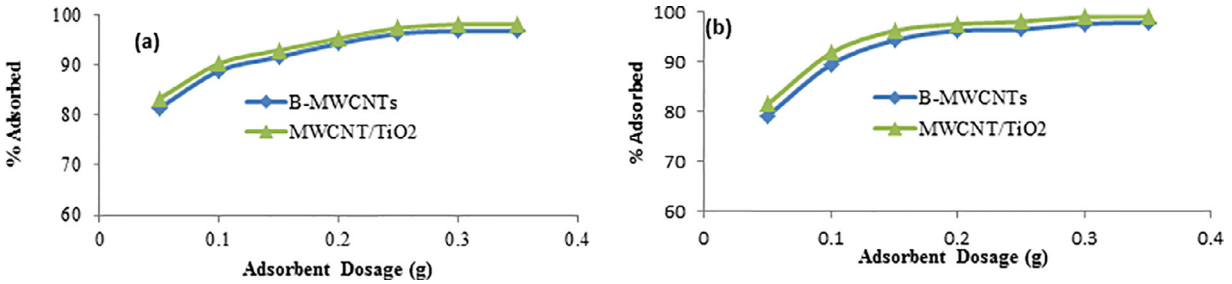

Fig. 17. Effect of adsorbent dosage on the percentage removal of (a) Cyanide and (b) Phenol onto MWCNTs and MWCNTs/TiO_2 nanodsorbents.

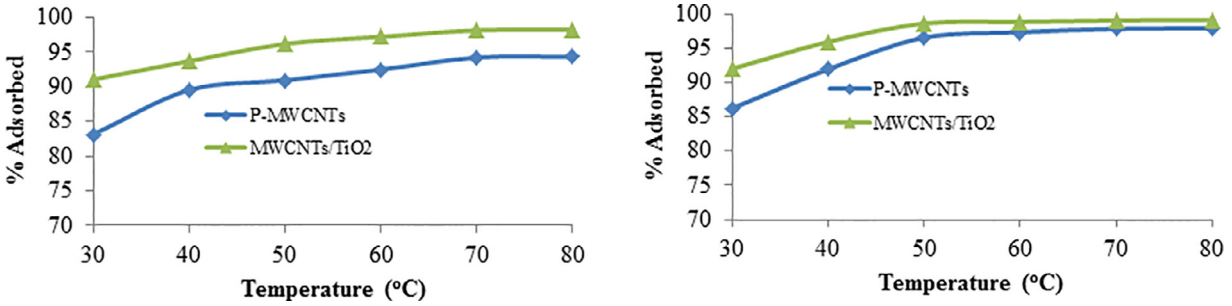

Fig. 18. Effect of temperature on the percentage removal of (a) Cyanide and (b) Phenol onto MWCNTs and MWCNTs/TiO_2 nanodsorbents.

the adsorption of phenol and cyanide onto the nanoadsorbent is not solely surface area dependent but rather on the surface functional group and material.

3.2. Results of the adsorption process

The effects of contact time, adsorbent dosage and temperature on the removal efficiency of phenol and cyanide are depicted in Figs. 16-18 respectively. The results show that the modification process improves the adsorption properties of the developed nanoadsorbent, MWCNTs/TiO_2. The effects of titanium oxide nanoparticles on the adsorption properties of MWCNTs for phenol and cyanide removal were noticeable. Table 2 shows the initial and final concentration of the refinery wastewater before and after treatment process.

From Fig. 16, it can be observed that the removal efficiency of both the cyanide and phenol by the nanoadsorbents increases with increasing contact time irrespective of the adsorbent. Also, at every contact time, the removal efficiency of MWCNTs/TiO_2 nanodsorbent is greater than the MWCNTs alone. This implies that the adsorption capacity of MWCNTs/TiO_2 > MWCNTs due to the presence of more functional groups in the former than the latter. In spite of the higher surface area

Table 4
Isotherm parameters for cyanide and phenol removal from refinery effluent using MWCNTs adsorbent

Pollutants	Isotherm	Parameters	Adsorbents	
			MWCNTs	MWCNTs/TiO_2
Phenol	Langmuir	K_L(L/mg)	0.072289	0.2775
		a_L(L/mg)	7.087172	15.949
		Q_o(mg/g)	98.03922	57.471
		R_L	0.13719	0.0398
		R^2	0.9692	0.9212
	Freundlich	K_f	8.01309	2.9988
		I/n	0.6951	0.6108
		n	1.438642	1.6372
		R^2	0.9038	0.9811
Cyanide	Langmuir	K_L(L/mg)	0.019873	0.1080
		a_L(L/mg)	2.288853	9.3110
		Q_o(mg/g)	12.0984	86.207
		R_L	0.88819	0.0790
		R^2	0.9437	0.9356
	Freundlich	K_f	1.75428	2.5922
		I/n	1.2232	0.7340
		n	0.817528	1.3624
		R^2	0.9734	0.9532

of the MWCNTs, the adsorption efficiency of the material was relatively low compared to MWCNTs/TiO_2 with slightly lower surface area. This indicates that the adsorption behaviour of the developed MWCNTs/TiO_2 is not completely surface area dependent but rather on the surface functional groups of the nanoadsorbent.

The Freundlich and Langmuir models were used to analyse the adsorption data in order to establish the most fitted model that best describe the adsorption process. The Freundlich and the Langmuir isotherms were determined using Eq. 8 and 9 respectively.

$$logq_e = logk_f + \frac{1}{n} logc_e \tag{8}$$

$$\frac{1}{qe} = \frac{1}{al} \cdot \frac{1}{Ce} + \frac{kl}{al} \tag{9}$$

Where q_e represents the equilibrium quantity that exists between the solid phase ion concentrations in the process (mg/L) while c_e is the equilibrium concentration in the liquid phase ion concentration (mg/L). The plot of log q_e against log c_e gives a very important information with the slope and intercept used to determine the constants of the Fraudlich model. In both cases, the correlation coefficient as well as the constant of the adsorption model were analysed and the results are shown in Table 4.

The Langmuir and the Freundlich isotherms are one of the major tools used in describing the nature of adsorption taking place between the adsorbate-adsorbent regimes. In Langmuir isotherm, a monolayer adsorption of adsorbate to the active pores of an adsorbent with no transmigration of adsorbates along the plane surface of the adsorbent is assumed. Immediately a site is filled-up, the model suggests that no further adsorption could take place at those particular sites. Hence, the surface and the pores are said to attain a saturation points; the point where the maximum adsorption of the sorbate is achieved.

From Table 4, R_L(separation factor) is a dimensionless parameter used for prediction of the affinity of sorbate and sorbent. The value of the separation factor indicates the nature of isotherm which a particular adsorption process fits. For an irreversible adsorption process (R_L=0), favourable (0>R_L<1), linear (R_L=0) and unfavourable (R_L>1). From the results depicted in Table 4, the value of the $R_L$for both the cyanide and phenol (0.88819 and 0.13719 respectively) onto the P-MWCNTs were both less than 1, this indicates that the adsorption process of the sorbates are favourable at the operating conditions.

Furthermore, the R^2 value is an important factor that predicts the best isotherm model that best described the fitting of the adsorption data. The adsorption of cyanide favours Freundlich isotherm (0.9734) than Langmuir (0.9437) because of it R^2 closer to unity. Hence, the agreement of the cyanide adsorption to the Freundlich isotherm model indicates that its adsorption to the surfaces and the active pores of the P-MWCNTs adsorbent is multilayer in nature. In contrary, the adsorption of phenol to the surface of the P-MWCNTs adsorbent obeys the Langmuir isotherm model due to high value of R^2 of 0.9692 which is closer to unity than that of the Freundlich isotherm model of 0.9038. The closer of the Langmuir R^2 to unity shows that the adsorption of phenol to the pore sites of the P-MWCNTs exhibit a monolayer adsorption nature.

The Q_o, maximum adsorption capacity was estimated from the Langmuir isotherm model for both the cyanide and phenol removal onto the active sites of the P-MWCNTs adsorbent. The highest maximum adsorption capacity was observed on phenol removal with a Q_o of 98.0392 mg/g while the lower values were observed for the cyanide removal with Q_o of 12.0984 mg/g for P-MWCNTs adsorbent. The deduction from the obtained value of Q_o is an indication that phenol has the

Table 5
Kinetic parameters for the removal of cyanide and phenol onto P-MWCNTs

Pollutants	Kinetics	Parameters	Adsorbents	
			MWCNTs	MWCNTs/TiO_2
Phenol	Pseudo-first order kinetic	q_e,exp (mg/g)	430.00	433.85
		q_e,cal (mg/g)	311.32	168.345
		k(min^{-1})	0.0684	0.0574
		R^2	0.9376	0.981
	Pseudo-second order kinetic	q_e,exp (mg/g)	430.00	433.85
		q_e,cal (mg/g)	454.55	423.45
		k(min^{-1})	0.000453	0.000756
		R^2	0.9996	0.999
	Elovic Model	β	0.0163	0.0264
		α	1067.99	55545.36
		R^2	0.9335	0.9261
Cyanide	Pseudo-first order kinetic	q_e,exp (mg/g)	509.95	533.95
		q_e,cal (mg/g)	100.462	171.91
		k(min^{-1})	0.0542	0.0634
		R^2	0.9226	0.7202
	Pseudo-second order kinetic	q_e,exp (mg/g)	509.95	533.95
		q_e,cal (mg/g)	526.316	555.56
		k(min^{-1})	0.000547	0.000661
		R^2	0.9984	0.9999
	Elovic Model	β	0.0152	0.0210
		α	2167.43	50432.35
		R^2	0.7611	0.9353

higher uptake than cyanide onto the active sites and surfaces of the P-MWCNTs. The effectiveness of the adsorbed cyanide and phenol were also examined by determining the binding strength which exists between the sorbate and the sorbent in solution. The binding strength, K_L is estimated from the Langmuir isotherm model. The highest binding strength was observed between the phenol and the P-MWCNTs adsorbent. Hence, cyanide was observed to occupy a less biding space than phenol on the active pores of the adsorbent. This could be the product of higher value of Q_o observed during the uptake of the phenol in the refinery wastewater.

The value of "n" as estimated from the Freundlich isotherm model is an indication that defines the adsorption characteristics of the adsorption process in relationship to the adsorbate. Several researchers have postulated the implication of "n" obtained from the Freundlich isotherm model. The value of n in the range of 1–10 points to the fact of the adsorption process is favourable. Also, the n values in the range of $2<n<10$ implies that the adsorption process is good, n value in the range of 1–2 means that the adsorption is relatively good and $n<1$ is an indication that the adsorption process is poor. From the results depicted in Table 4, the n values for cyanide is lower than 1, hence the adsorption characteristics is said to be poor.

For the adsorption of phenol and cyanide on to the synthesized MWCNTs/TiO_2 nano-adsorbent, the separation factor for both the cyanide and phenol were obtained to be0.0790 and 0.0398 respectively. The value of R_L less than unity is an indication that the adsorption process of the sorbates (cyanide and phenol) to the active pores of the sorbent is favourable at the operating conditions. The Langmuir and the Freundlich R^2 values for the removal of cyanide were 0.9356 and 0.9532 respectively on to the surfaces of the MWCNTs/TiO_2 nano-adsorbent. The closeness of the R^2 value of Freundlich model to unity shows that the adsorption of cyanide on to the sorbent is multilayer. Also, the closeness of the Freundlich R^2 of phenol to unity indicates that the adsorption of phenol to the pore sites of the MWCNTs/TiO_2 exhibits a multilayer adsorption. The highest maximum adsorption capacity was observed on cyanide removal with a Q_o of 86.207 mg/g while the lower value was observed for the phenol removal with Q_o of 57.471 mg/g. This result shows that cyanide has the higher uptake than phenol into the active sites and surfaces of the MWCNTs/TiO_2adsorbent from the refinery effluent. The reason to these could be due to the surface modification of the MWCNTs nano-material with titanium dioxide nanoparticles. Also, the binding strength estimated from the Langmuir isotherm model indicated that the highest binding strength was observed between the phenol and the MWCNTs/TiO_2adsorbent cyanide. The n-value estimated from the Freundlich isotherm model shows that the adsorption process for cyanide and phenol removal were favourable.

The kinetic models used for data fitting in this research study are the pseudo-first order, pseudo-second order and Elovich models and their relationships are shown in Eqs. 10, 11 and 12 respectively. The results of the kinetic models are as presented in Table 5.

$$\log(q_e - q_t) = \log q_e - \frac{K}{2.303}t \tag{10}$$

$$\frac{t}{q_t} = \frac{1}{k_2 q_e^2} + \frac{t}{q_e} \tag{11}$$

Table 6
Thermodynamic parameters of cyanide and phenol removal from refinery wastewater

Sorbent /Sorbate	Temp (°C)	$(\Delta H)^o$ (kJ/mol)	$(\Delta S)^o$ (kJ/mol)	$(\Delta G)^o$ (kJ/mol)
MWCNTs				
Cyanide	303	-19.0490	30.0794	-29.9811
	313			-30.3419
	323			-30.7027
	333			-31.0635
	343			-31.4243
	353			-31.7851
Phenol	303	-34.1564	77.8423	-57.7426
	313			-58.5211
	323			-59.2995
	333			-60.0779
	343			-60.8563
	353			-61.6487
MWCNTs/TiO_2	303	-26.8708	53.9695	-43.2236
Cyanide	313			-43.7633
	323			-44.2930
	333			-44.8427
	343			-45.3824
	343			-45.9221
Phenol	303	-38.5662	84.8942	-64.2891
	313			-65.1381
	323			-65.9870
	333			-66.8359
	343			-67.6849
	353			-68.5338

$$qt = \frac{1}{\beta e}\ln(\alpha\beta e) - \frac{1}{\beta e}lnt \tag{12}$$

Where k indicates the first order adsorption rate of the process ($L.min^{-1}$) extracted from the plot of log (q_e/q_t) against twhile the adsorption capacity (q_e).

The kinetic study of the removal of cyanide and phenol onto the P-MWCNTs and MWCNTs/TiO_2 nano-adsorbent were investigated and the results were as presented in Table 5. From the results obtained from the pseudo-first order kinetic model, the values for the q_e calculated and the estimated were far apart for the two adsorbents used in this study. The deduction from this variation in the equilibrium removal depicts that the removal of phenol and cyanide do not obey the pseudo-first order kinetic model. Corroboratively, the correlation coefficients, k as depicted from Table 5 shows that cyanide and phenol adsorption onto the surfaces of the adsorbents do not obey the pseudo-first order kinetic model. It was observed that the R^2 values for the pseudo-second order kinetic were closest to unity than that of the pseudo-first order kinetic and the Elovich models. This shows that the removal of cyanide and phenol on the surfaces and actives sites of the adsorbents obey the pseudo-second order kinetic model. The fitting of the adsorption model to the pseudo-second order kinetic indicates that the removal of the selected pollutants from the refinery wastewater is chemisorption in nature.

The thermodynamic parameters for the removal of cyanide and phenol from refinery wastewater by the P-MWCNTs and MWCNTs/TiO_2 sorbents are as depicted in Table 6 while Eqs. 13 and 14 represent the thermodynamic relationships.

$$\ln Kc = \frac{\Delta S}{R} - \frac{\Delta H}{RT} \tag{13}$$

$$\Delta G^\circ = \Delta H^\circ - T\Delta S^\circ \tag{14}$$

Where Kc represents the equilibrium constant, R is the gas constant (8.314 J/molK) while T is the absolute temperature in Kelvin. The data were fitted to generate the enthalpy, Gibb's free energy and entropy of the adsorption process for the respective adsorbent.

The result of the thermodynamic study for the removal of phenol and cyanide from the refinery wastewater were as depicted in Table 6. The enthalpy of the removal of cyanide and phenol were all negative. The negative values indicate the exothermic nature of the adsorption process which resulted to a strong bond formation between the cyanide and phenol to the surfaces and the active sites of the sorbent. The enthalpy of adsorption process was categorized to be physisorption when the value of $(\Delta H)^\circ$ falls within -20 t0 40 kJ/mol and chemisorption when it falls within -400 to -80 kJ/mol. Therefore, the adsorption of cyanide and phenol onto the P-MWCNTs and MWCNTs/TiO_2 adsorbents are physiosorption in nature. From the Table 6, the values for the entropies changes were positive in nature. The positive nature of the entropies depict that the adsorption process leading to the removal of cyanide and phenol on to the sorbents were not favoured at high temperature and hence, dissociative in nature. In addition, the positive values for the change in entropies indicate an increase in the

degree of freedom between the adsorbents and adsorbates leading to a weak interaction. The free energies change for the removal of phenol and cyanide were also investigated and the result shows that the values obtained were negative. The negative values of the free energies changes as depicted in Table 5 show that the adsorption process is spontaneous in nature.

4. Conclusions

The study investigates the development MWCNTs/TiO_2 as a novel adsorbent for the removal of phenol and cyanide from refinery wastewater via a batch adsorption process. To achieve this, the catalyst, Fe-Ni doped alumina was used for MWCNTs synthesis in a CVD reactor using acetylene as carbon source. The produced MWCNTs was purified using acid purification process to remove the accompanied metallic impurities. Titanium oxide nanoparticles were further produced via green synthesis technique then characterised for it surface properties. The kinetic, isotherm and thermodynamic of the adsorption process were then investigated. From the results obtained from various analyses conducted, the following conclusions are made:

1. The acid purification process adopted removes reasonable quantity of metallic and carbonaceous impurities from the as-synthesized MWCNTs.
2. Highly crystalline TiO_2 nanoparticles was produced without amorphous carbon accomplishment in an inert environment.
3. The highest maximum adsorption capacity was achieved on cyanide removal with a Q_o of 98.03922 mg/g.
4. The adsorption behaviour of the developed MWCNTs/TiO_2 is not completely surface area dependent but rather on the surface functional groups of the nanoadsorbent.
5. The adsorption of phenol and cyanide on to the adsorbents were all spontaneous in nature with favourable adsorption performance at elevated temperature.

Declaration of Competing Interest

The authors declare that they have no known competing financial interests or personal relationships that could have appeared to influence the work reported in this paper.

Acknowledgements

The financial support from the senate research based fund of Federal University of Technology, Minna with grant number (SENATE/FUTMINNA/2015/06) is much appreciated. Support received for the use of facilities at Centre for Genetic Engineering and Biotechnology, CGEB, Federal University of Technology, Minna, Nigeria is also acknowledged.

References

[1] C. Adams, Y. Wang, K. Loftin, M. Meyer, Removal of antibiotics from surface and distilled water in conventional water treatment processes, J. Environ. Eng. 128 (3) (2002) 253–260.
[2] A. Aliyu, A.S. Abdulkareem, A.S. Kovo, O.K. Abubakre, J.O. Tijani, I. Kariim, Synthesize multi-walled carbon nanotubes via catalytic chemical vapour deposition method on Fe-Ni bimetallic catalyst supported on kaolin, Carbon Lett. 21 (2017) 33–50.
[3] A. Ansón-Casaos, I. Tacchini, A. Unzue, M.T. Martínez, Combined modification of a TiO_2 photocatalyst with two different carbon forms, Appl. Surf. Sci. 270 (2013) 675–684.
[4] F. Bani, M. John, A.F.A. Sharfudeen, V.A. Rose, J. Pharm. Sci. Res. 9 (9) (2017) 1604–1608.
[5] S. Cataldo, A. Gianguzza, D. Milea, N. Muratore, A. Pettignano, Pb(II) adsorption by a novel activated carbon- alginate composite material. A kinetic and equilibrium study, Int. J. Biol. Macromol. 92 (2016) 769–778.
[6] M. Falkenmark, Water resilience and human life support - global outlook for the next half century, Int. J. Water Resour. Dev. 36 (2-3) (2020) 377:396.
[7] M.H. Fatehi, J. Shayegan, M. Zabihi, I. Goodarznia, Functionalized magnetic nanoparticles supported on activated carbon for adsorption of Pb(II) and Cr(VI) ions from saline solutions, J. Environ. Chem. Eng. 3 (2017) 1–31.
[8] P.K. Gautam, R.K. Gautam, S. Banerje, M.C. Chattopadhyaya, J.D. Pandey, Heavy Metals in the Environment: Fate, Transport, Toxicity and Remediation Technologies, Nava Science Publishers, Inc, 2016 ISBN: 978-1-63484-740-7.
[9] Hossein D. Atoufi, David J. Lampert, Impacts of oil and gas production on contaminant levels in sediments, Curr. Pollut. Report 6 (2020) 43–53 https://doi.org/10.1007/s40726-020-00137-5.
[10] I. Ilaboya, E. Oti, G. Ekon, L. Umukoro, Performance of activated carbon from cassava peels for the treatment of effluent wastewater, Iranica J. Energy Environ. 4 (4) (2013) 361–371.
[11] M.S. Kuyukina, A.V. Krivoruchko, I.B. Ivshina, Advanced bioreactor treatments of hydrocarbon-containing wastewater, Appl. Sci. 2020 (10) (2020) 831.
[12] P.S. Leonard, J. Hearty, S. Brennan, Advances in biosensors for detection of pathogens in food and water, Enzyme Microb. Technol. 32 (1) (2003) 3–13.
[13] P.M. Masipa, T. Magadzu, B. Mkhondo, Decoration of multiwalled carbon nanotubes by metal nanoparticles and metal oxidesusing chemical evaporation method, S. Afr. J. Chem. 66 (2013) 173–178.
[14] Y.S. Mohammad, R.M. Shuaibu-Imodagbe, S.B. Igboro, A. Giwa, C.A. Okuofu, Adsorption of phenol from refinery wastewater using rice husk activated carbon, Iranica J. Energy Environ. 5 (4) (2014) 393–399.
[15] E.T. Mombeshora, R. Simoyi, V.O. Nyamori, S. Ndungu, Multiwalled carbon nanotube-titania nanocomposites: understanding nano-structural parameters andfunctionality in dye-sensitized solar cells, Afr. J. Chem. 68 (2015) 153–164.
[16] V.O. Njoku, Biosorption potential of coca pod husk for the removal of Zn(II) from aqueous phase, J. Environ. Chem. Eng. 2 (2014) 881–887.
[17] S. Nora, S.D. Mamadou, Nanomaterials and water purification: opportunities and challenges, J. Nanopart. Res. 7 (2005) 331–342.
[18] B.C. Nyamunda, Review of the impact on water quality and treatment options of cyanide used in gold ore processing, Water Quality, IntechOpen, Hlanganani Tutu, 2017 DOI: 10.5772/65706Available from: https://www.intechopen.com/books/water-quality/review-of-the-impact-on-water-quality-and-treatment-options-of-cyanide-used-in-gold-ore-processing .
[19] K.S. Padmavathy, G. Madhu, P.V. Haseena, A study on effects of pH, adsorbent dosage, time, initial concentration and adsorption isotherm study for the removal of hexavalent chromium (Cr (VI)) from wastewater by magnetite nanoparticles, Proc. Technol. 24 (2016) 585–594.

[20] A.L. Peigney, F. Christophe, B. Emmanuel, R.A. Revathi, Specific surface area of carbon nanotubes and bundles of carbon nanotubes, Carbon 39 (4) (2001) 507–514.
[21] Z. Peining, A.S. Nair, Y. Shengyuan, P. Shengjie, N.K. Elumalai, S. Ramakrishna, Rice grain-shaped TiO_2-CNT composite – a functional material with a novel morphology for dye-sensitized solar cell, J. Photochem. Photobiol.A 231 (2012) 9–18.
[22] J. Pichtel, Oil and gas production wastewater: soil contamination and pollution prevention, Appl. Environ. Soil Sci 2016 (2016) Article ID 2707989 http://dx.doi.org/10.1155/2016/2707989 .
[23] K.G. Rao, K. Ashok, V. Rao, S. Vhakra, V. Rajendar, Synthesis of TiO_2 nanoparticles from orange fruit waste, Int. J. Multidis. Adv. Res. Trends 2 (1) (2015) 82–90.
[24] K Thamaphat, P Limsuwan, B Ngotawornchai, Phase characterization of TiO2 powder byXRD and TEM, Kasetsart. J. (Nat. Sci.) 42 (2008) 357–361.
[25] A Tripathi, M.R. Ranjan, Heavy metal removal from wastewater using low cost adsorbents, J. Bioremed. Biodegrad. 6 (6) (2015) 315–319 http://dx.doi.org/, doi:10.4172/2155-6199.1000315.
[26] K.R. Walha, B. Amar, L. Firdaous, F. Quem´eneur, P. Jaouen, Ḃrackish groundwater treatment by nanofiltration, reverse osmosis and electrodialysis in Tunisia: performance and cost comparison, Desalination 207 (1–3) (2007) 95–106.